Astron. Astrophys. 355, 406–412 (2000)

ASTRONOMY AND ASTROPHYSICS

Resonant inverse Compton scattering by secondary pulsar plasma

Y.E. Lyubarskii and S.A. Petrova

Institute of Radio Astronomy, Chervonopraporna St.4, Kharkov, 310002 Ukraine

Received 22 July 1999 / Accepted 7 December 1999

Abstract. We consider resonant inverse Compton scattering of thermal photons by secondary particles above the pulsar polar gap. At neutron star temperatures higher than 10^5 K the process appears to be an essential energy loss mechanism for the particles. The distribution function of the secondary plasma particles is found to be strongly affected by the scattering. It becomes two-humped implying the development of two-stream instability. The resonantly upscattered Compton photons are found to gain energy of 1–10 MeV forming an additional component in the pulsar gamma-ray spectrum. The corresponding gamma-ray flux is estimated as well.

Key words: plasmas – scattering – stars: pulsars: general – gamma rays: theory

1. Introduction

Rotation of a highly magnetized neutron star is known to induce a strong electric field, which intensely accelerates charged particles. According to the customary polar gap models (Ruderman & Sutherland 1975, Arons & Scharlemann 1979), the acceleration takes place near the neutron star surface above the polar cap, the Lorentz-factor of the primary particles increasing up to $\sim 10^6$. The particles move along the magnetic lines and emit curvature photons, which initiate pair-production cascade. The first electron-positron pairs created screen the accelerating electric field, so that at higher altitudes the particle energy remains unaltered; the typical Lorentz-factors of the secondary plasma are $\sim 10 - 10^4$.

Recent observations testify to thermal soft X-ray emission from some pulsars indicating that the neutron stars can be rather hot, $T \sim 5{\cdot}10^5$ K, while the polar caps can have still higher temperatures scaling a few times 10^6 K (Cordova et al. 1989, Ogelman 1991, Halpern & Holt 1992, Finley et al. 1992, Halpern & Ruderman 1993, Ogelman & Finley 1993, Ogelman et al. 1993, Yancopoulos et al. 1994, Ogelman 1995, Greiveldinger et al. 1996). Such high temperatures of the neutron star surface are also predicted theoretically (Alpar et al. 1984, Shibazaki & Lamb 1989, Van Riper 1991, Page & Applegate 1992, Umeda et al. 1993, Halpern & Ruderman 1993). The thermal X-ray photons should suffer inverse Compton scattering off the primary particles in the polar gap. In the presence of a strong magnetic field the scattering cross-section is essentially enhanced, if the photon energy in the particle rest frame equals the cyclotron energy (Herold 1979, Xia et al. 1985). For the pulsars with hot polar caps the resonant Compton scattering in the polar gap was found to be rather efficient (Kardashev et al. 1984, Xia et al. 1985, Daugherty & Harding 1989, Dermer 1990, Sturner 1995, Chang 1995). Firstly, it was recognized as an essential mechanism for energy loss of primary particles accelerating in the polar gap. Secondly, inverse Compton scattering was found to condition the gap formation, since the pair production avalanche may be triggered by the upscattered Compton photons rather than by curvature photons (Zhang & Qiao 1996, Qiao & Zhang 1996, Luo 1996, Zhang et al. 1997).

As shown by Sturner (1995), given typical values of neutron star temperature and surface magnetic field, the resonant Compton scattering is the strongest for particle Lorentz-factors $\sim 10^2 - 10^3$. Theoretical models (Van Riper 1991, Page & Applegate 1992, Umeda et al. 1993) suggest that the typical temperatures of the neutron star surface are as high as a few times 10^5 K. Hence, the scattering is likely to be essential for the secondary plasma in most of the pulsars. Daugherty & Harding (1989), Zhang et al. (1997) traced the evolution of the Lorentz-factor of secondary particles on account of magnetic inverse Compton scattering above the polar gap. Our aim is to investigate in more detail the influence of resonant inverse Compton scattering on the parameters of secondary plasma. For the resonant character of the scattering, the evolution of particle Lorentz-factor with the distance depends strongly on the initial particle energy. Since the distribution function of the secondary plasma is generally believed to be rather broad (the Lorentz-factor ranges from 10 to 10^4), its evolution on account of the Compton scattering is of a great interest. It will be shown that only particles with Lorentz-factors between 100 and 1000 are essentially decelerated in the course of the resonant scattering forming a sharp peak at low energies. Particles with larger Lorentz-factors are not decelerated at all. Thus, the resultant distribution function of secondary particles becomes two-humped, giving rise to the two-stream instability.

In Sect. 2 we examine how the resonant inverse Compton scattering affects the Lorentz-factor of a secondary particle at various pulsar parameters. Sect. 3 is devoted to studying the

evolution of the distribution function. The conditions for the development of the two-stream instability are also discussed. In Sect. 4 we estimate the gamma-ray luminosity caused by the upscattered Compton photons. Sect. 5 contains a brief summary.

2. Deceleration of secondary particles due to resonant inverse Compton scattering

Consider the flow of secondary plasma streaming along the open magnetic field lines above the polar gap. The neutron star is supposed to emit a blackbody radiation, which is scattered by the plasma particles. In a strong magnetic field the scattering is particularly efficient, if the photon energy, εmc^2, satisfies the resonance condition:

$$\varepsilon\gamma(1-\beta\cos\theta)=\varepsilon_B, \tag{1}$$

where γ is the Lorentz-factor of the scattering particles, β the particle velocity in units of c, θ the angle the photon makes with the particle velocity, $\varepsilon\equiv B/B_{cr}$, with $B_{cr}=m^2c^3/\hbar e=4.414\cdot10^{13}$ G. At the distance z from the neutron star the rate of energy loss due to the resonant inverse Compton scattering can be written as (Sturner 1995):

$$\frac{d\gamma}{dt} = 4.92\cdot10^{11}\frac{T_6B_{12}^2(z)}{\beta\gamma} \times\ln\left[1-\exp\left(-\frac{\varepsilon_B mc^2}{\gamma(1-\beta\cos\theta_c(z))kT}\right)\right]\mathrm{s}^{-1}. \tag{2}$$

Here T_6 is the neutron star temperature in units of 10^6 K, $B_{12}(z)$ the magnetic field strength in units of 10^{12} G, $\theta_c(z)$ the maximum incident angle of photons,

$$\cos\theta_c=\sqrt{1-\frac{1}{(1+z/R)^2}}, \tag{3}$$

where R is the neutron star radius. Provided that the magnetic field is dipolar, $B_{12}(z)\propto(1+z/R)^{-3}$.

Numerical solutions of Eq. (2) are presented in Fig. 1. One can see that the resonant inverse Compton scattering is significant up to $z\sim R$ and it affects the particle Lorentz-factor essentially. Note that the curves for different initial Lorentz-factors are not similar to each other. In agreement with Eq. (1), the larger the particle Lorentz-factor the lower is the energy of resonantly scattered photons. At $\gamma_0=3000$ the energy of the resonant photons is below $\varepsilon_{max}=2.82kT/(mc^2)$, which corresponds to the maximum in the photon distribution. As γ is decreasing with the altitude, the resonant energy increases. Hence, the photon spectral density increases and the scattering becomes more efficient. However, at distances $z\sim R$ it ceases due to the essential shrinking of the solid angle subtended by the neutron star. If the initial Lorentz-factor is 100, the energy of resonant photons is above ε_{max} and further increases with the altitude, so that the scattering gradually ceases.

Theoretical models predict that the polar cap region should be significantly hotter than the rest surface of the neutron star (e.g. Cheng & Ruderman 1980, Arons 1981, Alpar et al. 1984, Umeda et al. 1993, Luo 1996). However, the luminosities observed from the hot spots appear to be too small (Finley et al. 1992, Halpern & Ruderman 1993, Becker & Trumper 1993, Yancopoulos et al. 1994, Greiveldinger et al. 1996). The latter is usually interpreted as a consequence of small hot spot radii (e.g. Yancopoulos et al. 1994, Greiveldinger et al. 1996). As is evident from Fig. 1, for typical hot spot parameters the particle energy loss is mainly determined by the scattering of the photons from the whole neutron star rather than by the scattering of hot spot photons. So hereafter we take into account only the photons from the whole neutron star surface keeping in mind that the influence of hot spot photons can somehow alter our quantitative results, while the qualitative picture should remain the same.

It should be pointed out that the evolution of Lorentz-factor with the altitude shown in Fig. 1 is somewhat different from that reported by Zhang et al. (1997) (see their Fig. 1). These authors claim that at distances $z\lesssim10R$ the particles suffer severe non-

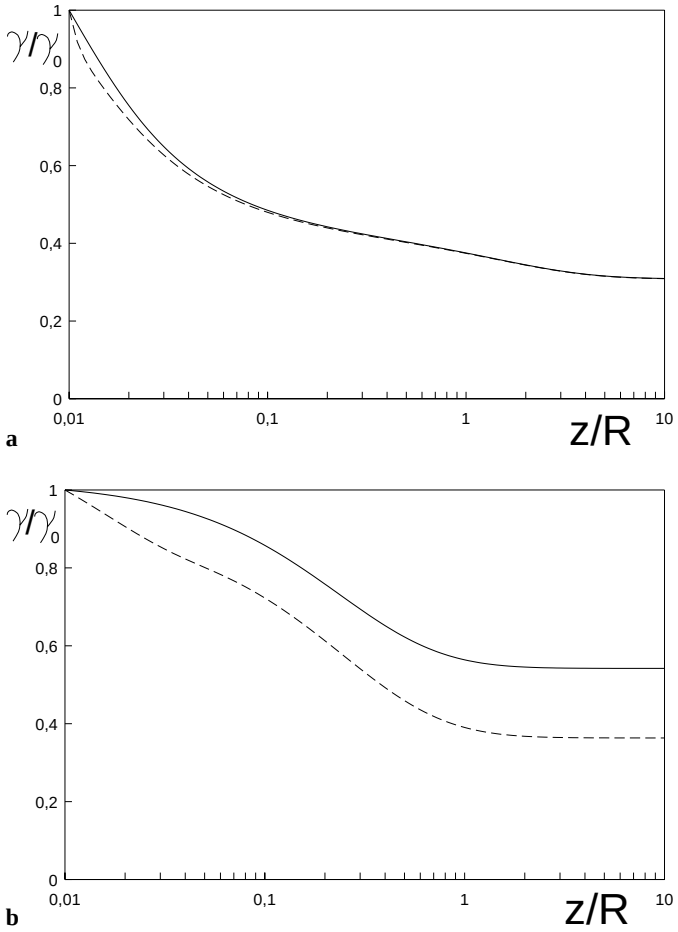

Fig. 1a and b. Evolution of particle Lorentz-factor with the distance for initial Lorentz-factors, $\gamma_0=100$ **a** and $\gamma_0=3000$ **b**; $B_{12}=1$, $z_0/R=0.01$.The solid lines are plotted for the case of scattering the photons from the whole neutron star surface with the temperature $5{\cdot}10^5$K, whereas the dashed lines refer to the case when the contribution of the hot spot photons is also taken into account(here the hot spot radius is $5\cdot10^{-3}R$ and the temperature is $3\cdot10^6$K).

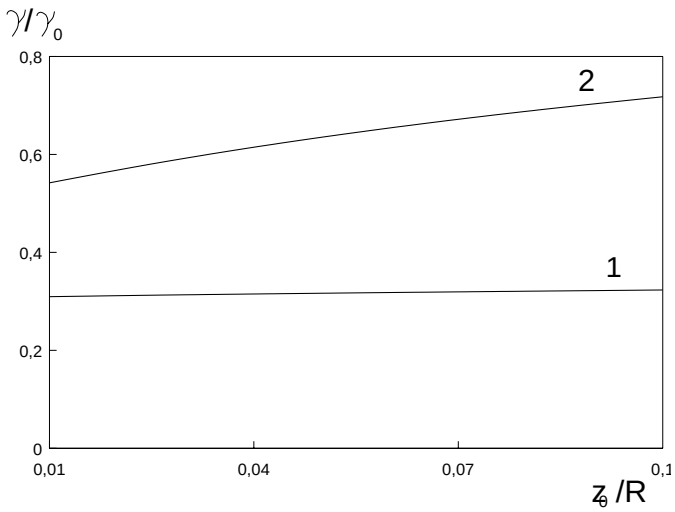

Fig. 2. Final Lorentz-factor versus the gap height for $\gamma_0 = 100$ (curve 1) and $\gamma_0 = 3000$ (curve 2); $T_6 = 0.5$, $B_{12} = 1$

resonant magnetized scattering, which leads to the drastic decrease of the final Lorentz-factor. In fact, the rate of energy loss on account of nonresonant magnetic scattering increases with decreasing the field strength as $B_{12}^{-2}(z)$ (see Eq. (5) in Sturner 1995). However, this equation is applicable only if in the particle rest frame the cyclotron energy exceeds the energy of most of photons, $\varepsilon_B > \varepsilon\gamma(1 - \beta\cos\theta_c)$. For the photon energies at the peak of the Planck distribution, $\varepsilon \approx 2.82kT$, the latter condition can be rewritten as $4 \cdot 10^{-2} B_{12}(z)/(T_6\gamma_3(1 - \beta\cos\theta_c)) > 1$, with $\gamma_3 \equiv \gamma/10^3$. Taking $T_6 = 0.5$, $\gamma_3 = 3$, $B_{12} = 0.1$ (Zhang et al. 1997, Fig. 1a), one can obtain that at $z = 10R$ the left-hand side of this inequality is $5 \cdot 10^{-5}$, while at $z = 0$ it equals $3 \cdot 10^{-4}$. So even at the stellar surface most of the photons scatter in the Thomson regime rather than in the magnetic one. The rate of energy loss out of the Thomson scattering is found to be

$$\frac{d\gamma_T}{dt} = -30\gamma T_6^4 (1 - \beta\cos\theta_c)^3 \,\mathrm{s}^{-1}, \qquad (4)$$

showing that this process is inefficient. Thus the resonant inverse Compton scattering is the only significant energy loss mechanism for the secondary particles in pulsar magnetospheres.

We believe that the particles start deceleration just above the polar gap. In general the gap thickness is supposed to be of the order of the polar cap radius (Ruderman & Sutherland 1975) or even larger (Arons & Scharlemann 1979). The energy loss of secondary particles due to the resonant inverse Compton scattering above the gap should certainly be influenced by the adopted value of the gap height. In Fig. 2 we show the final Lorentz-factors versus the gap height. One can see that the dependence is sufficiently weak, therefore, below we fix z_0 at $10^{-2}R$.

In contrast with the gap height, such pulsar parameters as the star temperature and magnetic field strength can influence particle deceleration essentially. In Fig. 3 we present the dependences of the normalized final Lorentz-factor on the neutron star temperature at various magnetic field strengths. Apparently, at the temperatures $< 10^5$ K the scattering is inefficient yet, while

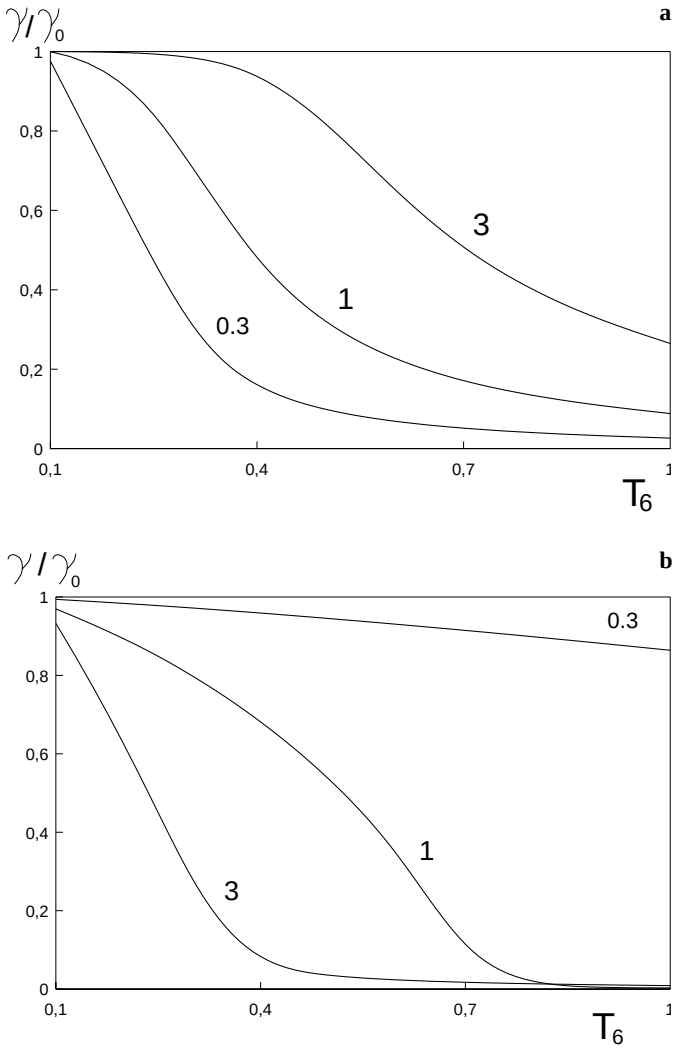

Fig. 3a and b. Final Lorentz-factor versus the temperature for various magnetic field strengths, B_{12}: **a** $\gamma_0 = 100$, **b** $\gamma_0 = 3000$

at higher temperatures it becomes significant. Note that at various initial Lorentz-factors ($\gamma_0 = 100$ and 3000) the scattering efficiency versus magnetic field strength is essentially different. The particles with $\gamma_0 = 100$ resonantly scatter the photons from the Wien region. Then the weaker the field strength, the lower is the energy of resonant photons and, correspondingly, the higher is the photon spectral density and the larger is the particle energy loss (see Fig. 3a). At $\gamma_0 = 3000$ the resonant energy lies in the Rayleigh-Jeans region. So the scattering is more efficient for higher magnetic field strengths, since the photon spectral density increases with the energy (see Fig. 3b).

For the resonant character of the scattering the particle energy loss depends strongly on the initial Lorentz-factor. Fig. 4 shows the final Lorentz-factor versus the initial one for various neutron star temperatures and magnetic field strengths. At $\gamma_0 \sim 10$ as well as at $\gamma_0 \sim 10^4$ the resonant scattering appears to be inefficient. Provided that the scattering is intense ($\gamma_0 \sim 10^2 - 10^3$), the final Lorentz-factor appears to be independent of the initial one. According to Fig. 4a, the length of the

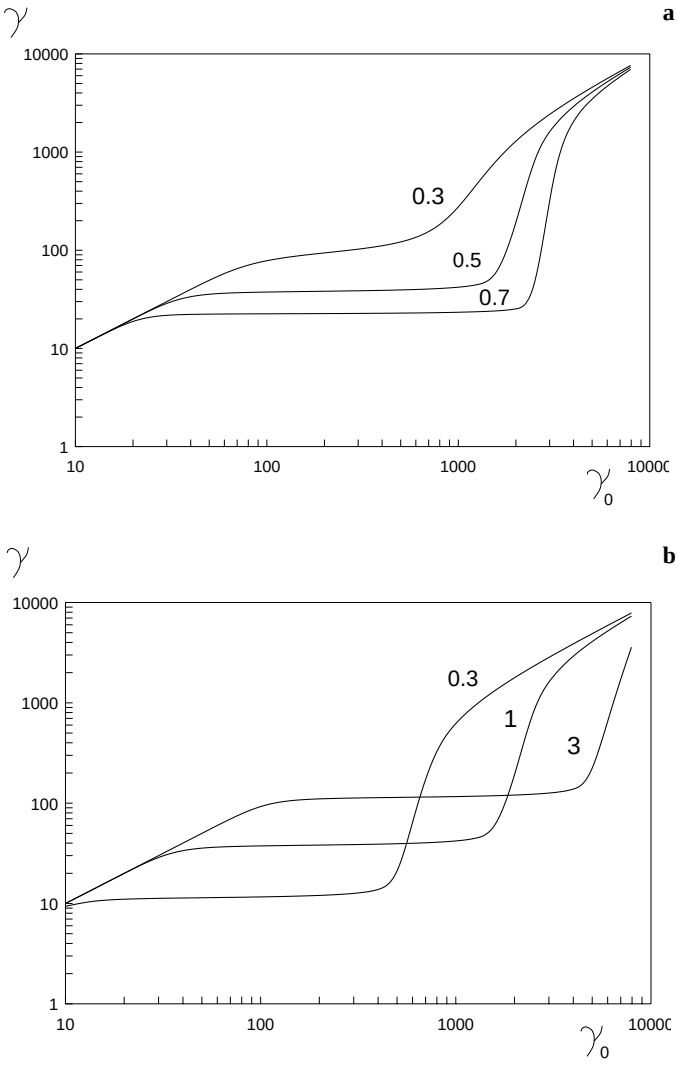

Fig. 4a and b. Final Lorentz-factor versus the initial one: **a** for various temperatures, T_6; $B_{12} = 1$, **b** for various magnetic field strengths, B_{12}; $T_6 = 0.5$

plateau increases with the star temperature. In fact, the higher temperature implies the larger amount of photons at every energy, the scattering becoming more efficient. As can be seen from Fig. 4b, the increase of the magnetic field strength leads to the shift of the plateau toward a higher energy; this is certainly consistent with the resonance condition (1).

3. The distribution function of the secondary plasma as a result of resonant inverse Compton scattering

Since the energy loss depends essentially on the initial particle energy, we are to investigate the evolution of the distribution function of secondary particles as a result of the resonant inverse Compton scattering. Conservation of the number of particles along a phase trajectory implies that

$$f(z,\,\gamma)d\gamma = f(z_0,\,\gamma_0)d\gamma_0\,,$$

where $f(z,\,\gamma)$ is the particle distribution function and the subscript "0" refers to the initial values. So looking for the phase trajectories of individual particles one can reconstruct the distribution function at any height z. We are particularly interested in the final distribution function arising at distances, where the resonant scattering ceases.

Let us begin with the evolution of a waterbag distribution function:

$$f(z_0,\,\gamma_0) = \begin{cases} \frac{1}{\gamma_{max}-\gamma_{min}}, & \gamma_{min} \le \gamma \le \gamma_{max}, \\ 0\,, & \gamma < \gamma_{min}\,\text{and}\,\gamma > \gamma_{max}, \end{cases}$$

with $\gamma_{min} = 10$, $\gamma_{max} = 10^4$. The final distribution functions at various pulsar parameters are plotted in Fig. 5. The particles with $\gamma \sim 10^2 - 10^3$ are essentially decelerated due to the scattering, the final energies becoming equal (see also Fig. 4). These particles form the sharp peak at $\gamma < 10^2$. For the Lorentz-factors of a few thousand the scattering becomes inefficient and the distribution function remains almost unaltered. Thus, the resonant inverse Compton scattering leads to the two-humped distribution function of the secondary plasma. At higher neutron star temperatures the main peak of the function shifts towards the lower energies and the humps become more prominent. The magnetic field strength variation also results in the shift of the main peak. For the more realistic distribution function resembling that found by Arons (1980),

$$f(\gamma) = \begin{cases} \exp\left(-10\frac{\gamma_m-\gamma}{\gamma_m}\right), & 10 \le \gamma \le \gamma_m, \\ (\gamma/\gamma_m)^{-3/2}, & \gamma_m \le \gamma \le \gamma_c, \\ (\gamma_c/\gamma_m)^{-3/2}\exp\left(-\frac{\gamma-\gamma_c}{\gamma_c}\right), & \gamma_c \le \gamma \le 10^4, \end{cases} \quad (5)$$

with $\gamma_m = 10^2$, $\gamma_c = 10^{3.5}$, the evolution on account of the resonant inverse Compton scattering is qualitatively the same (see Fig. 6).

We next examine the dispersion properties of the plasma with the evolved distribution function. For simplicity let us assume that the plasma consists of the two particle flows characterized by the number densities n_a, n_b and by the Lorentz-factors γ_a, γ_b ($\gamma_a < \gamma_b$). Given the infinitely strong magnetic field, the dispersion relation is as follows (see, e.g. Lyubarskii 1995):

$$\frac{\omega_{pa}^2}{(\omega - kv_a)^2\gamma_a^3} + \frac{\omega_{pb}^2}{(\omega - kv_b)^2\gamma_b^3} = 1. \quad (6)$$

Here ω is the frequency, k the wave number, $v_{a,b}$ are the particle velocities, $\omega_{pa,b}$ the plasma frequencies given by the customary expression:

$$\omega_{pa,b} = \sqrt{\frac{4\pi n_{a,b}e^2}{m}}, \quad (7)$$

where e is the electron charge, m the electron mass. As is evident from Eq. (6), the dispersion properties of the plasma are mainly determined by one of the particle flows on condition that

$$\frac{n_a}{\gamma_a^3} \gg \frac{n_b}{\gamma_b^3}, \quad (8)$$

rather than $n_a \gg n_b$. This is because of the great inertia of the fast particles performing one-dimensional motion in the superstrong magnetic field. For the distribution functions plotted

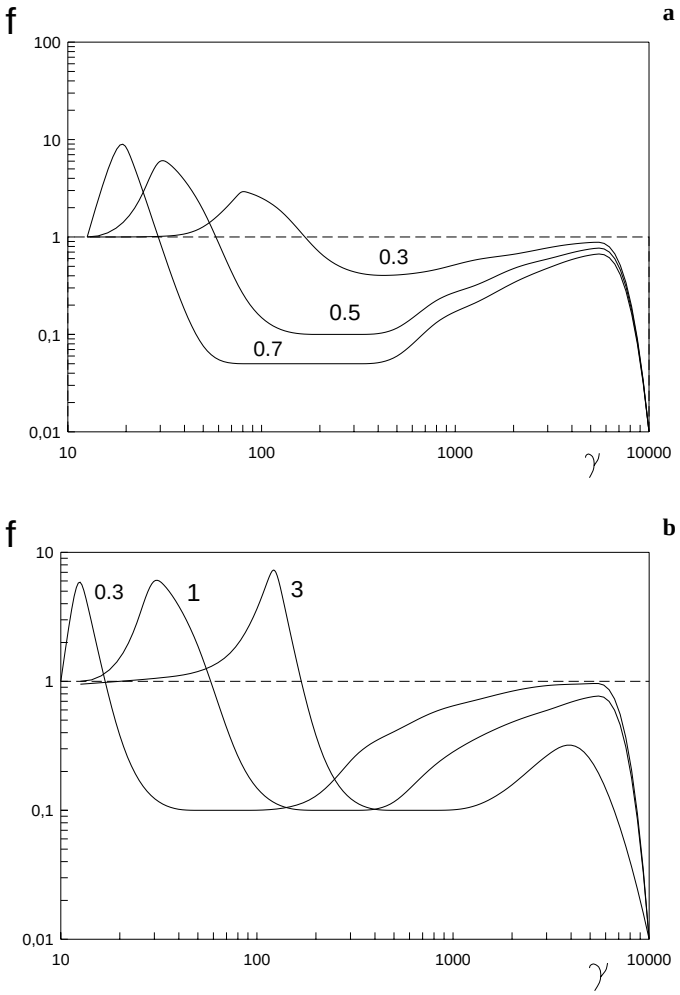

Fig. 5a and b. Evolution of the waterbag distribution function on account of resonant inverse Compton scattering: **a** for various temperatures, T_6; $B_{12} = 1$, **b** for various magnetic field strengths, B_{12}; $T_6 = 0.5$; the initial distribution function is shown by the dashed line

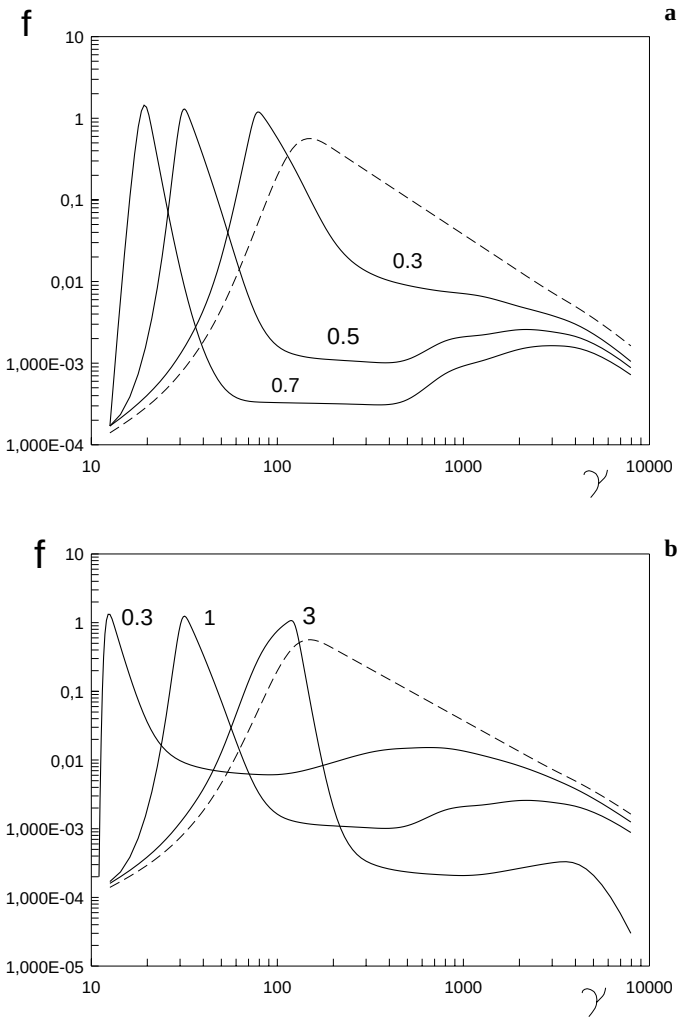

Fig. 6a and b. The same as in Fig. 5 for the initial distribution function (5)

in Figs. 5 and 6 n_a and n_b are comparable, while $\gamma_a/\gamma_b \sim 10^{-1} - 10^{-2}$. Therefore the low-energy particles of the main peak almost completely determine the dispersion properties of the plasma.

The two-humped distribution function implies the possibility of the two-stream instability. Provided that the contribution of one of the plasma flows to the plasma dispersion is small (*i.e.* Eq. (8) is valid), the growth rate of the instability takes the form (Lominadze & Mikhailovskii 1979, Cheng & Ruderman 1980):

$$\Im\omega \approx \left(\frac{n_b}{n_a}\right)^{1/3} \frac{\omega_{pa}}{\gamma_a^{1/2}\gamma_b}. \tag{9}$$

The two-stream instability results in an essential development of initial perturbations on condition that

$$\frac{R_c}{c}\Im\omega \gtrsim 10, \tag{10}$$

where R_c is the characteristic scale length for the increase of perturbations.

It is convenient to normalize the number density of the secondary plasma by the Goldreich-Julian charge density:

$$n = \frac{\kappa B}{Pce}, \tag{11}$$

where κ is the multiplicity factor of the secondary plasma, P the pulsar period. The latter equation can be rewritten as:

$$n = 6.25 \cdot 10^{13} P^{-1} \kappa_3 B_{12} (1 + z/R)^{-3}\,\mathrm{cm}^{-3}, \tag{12}$$

where $\kappa_3 \equiv \kappa/10^3$. Using Eqs. (9) and (12) in Eq. (10) we reduce the condition for the efficient instability development to the form:

$$\frac{\kappa_3 B_{12}}{P R_{c7} \gamma_{b3}^2 \gamma_{a2}} > 4 \cdot 10^{-4}. \tag{13}$$

Here $R_{c7} \equiv R_c/10^7\mathrm{cm}$, $\gamma_{b3} \equiv \gamma_b/10^3$, $\gamma_{a2} \equiv \gamma_a/10^2$ and it is assumed that $(n_b/n_a)^{1/3} \approx 1$. As can be seen from Eq. (13), at typical pulsar parameters the two-stream instability can develop readily providing the increase of plasma oscillations. The latter can be transformed into electromagnetic waves, thus giving rise to pulsar radio emission.

It should be mentioned that two-steram instability has always been one of the most popular mechanisms for pulsar radio emission. For more than two decades a number of scenarios for the instability development were proposed. The first and the most natural one involves the instability caused by the flows of primary and secondary pulsar plasma (Ruderman & Sutherland 1975). However, the growth rate of this instability appears to be too small because of enormous inertia of the high-energy primary particles (Benford & Buschauer 1977). Cheng & Ruderman (1977) considered the two-stream instability arising in the secondary plasma due to the difference in the velocities of electrons and positrons moving along the curved magnetic lines. However, this difference is insufficient to cause the instability, since the particle distribution functions are too broad (Buschauer & Benford 1977). Lyubarskii (1993) suggested that current and number density adjustment in pulsar magnetosphere leads to the backward particle flow, which causes intense two-stream instability. However, numerical simulations of the plasma flow in the open field line tube are necessary to prove this idea. Given nonstationary generation of the secondary plasma the particles are confined to the separate clouds, and the fastest particles of a cloud can outstrip the slower particles of the previous cloud giving rise to the two-stream instability (Usov 1987, Ursov & Usov 1988). Up to now it is not clear whether the instability initiated in such a way can account for pulsar radio emission, since the nonstationarity of plasma generation is not studied in detail yet. The present paper suggests one more possibility of two-stream instability in pulsars, which is based on the selective energy loss of particles as a result of resonant inverse Compton scattering. Note that in this model the instability arises naturally, with no additional assumptions being involved.

4. Gamma-ray luminosity provided by resonantly upscattered Compton photons

The photons produced by the resonant inverse Compton scattering have the energies

$$E \sim \gamma \epsilon_B mc^2 \sim B_{12}\gamma_2 \,\mathrm{MeV}, \tag{14}$$

so that typically $E \sim 1 - 10$ MeV. Note that the curvature gamma-photons produced in the polar gap as well as the photons upscattered by the primary particles have essentially higher energies, $E \gtrsim 100$ MeV. Hence, the resonant scattering by secondary plasma results in an additional low-energy component in pulsar gamma-ray spectrum. The spectrum of this component in the case of some specific distribution functions of the scattering particles is obtained by Daugherty & Harding (1989). In general, the low-energy tail of this component spreads even to the X-ray band on account of the photons resonantly scattered at distances $z > R$, where the magnetic field strength decreases essentially. However, these photons are very few, since at $z > R$ the scattering rate decreases significantly due to the shrinking of the solid angle subtended by the neutron star.

Given that the scattering is efficient, most of the energy of the secondary plasma should be transferred to the low-energy gamma-rays. The luminosity provided by the upscattered photons can be estimated as follows:

$$L = nSmc^3\Delta\gamma, \tag{15}$$

where S is the cross-sectional area of the open field line tube,

$$S = \frac{\pi R^3}{R_L}, \tag{16}$$

R_L is the light cylinder radius, $\Delta\gamma$ the difference between the Lorentz-factors of the particles, which mainly contribute to the final and initial plasma energy, $\Delta\gamma \sim 10^2 - 10^3$. Substituting Eqs. (12) and (16) into Eq. (15) we find:

$$L = 0.942 \cdot 10^{30} \frac{B_{12}R_6^3\kappa_3\gamma_3}{P^2}\,\mathrm{ergs/s}. \tag{17}$$

Although in the particle rest frame the photons are scattered in all directions, in the laboratory frame they are beamed along the particle velocity. So the opening angle of the gamma-ray beam is given by $\varphi = 3\sqrt{R/R_L}$. The averaged observed photon flux, F, is related to the luminosity as

$$F = \frac{L\varphi}{2\pi\Omega d^2 E\Delta E}, \tag{18}$$

where $\Omega = \pi\varphi^2/4$ is the solid angle occupied by the beam of upscattered photons, d the distance to the pulsar, ΔE the energy band. Taking into account Eq. (17), Eq. (18) can be rewritten as

$$F = 3 \cdot 10^{-10} \frac{B_{12}R_6^{5/2}\gamma_3\kappa_3}{P^{3/2}d_3^2E_6^2}\,\mathrm{photons/(cm^2 \cdot s \cdot keV)}, \tag{19}$$

where $d_3 \equiv d/10^3\,\mathrm{pc}$, $E_6 \equiv E/1\,\mathrm{MeV}$.

For most pulsars the flux given by Eq. (19) is too low to be detected. At present the detectors of the Compton gamma-ray observatory are the most sensitive to the low-energy gamma-ray emission (OSSE at 0.05–10 MeV and COMPTEL at 1–30 MeV). At 1 MeV the source sensitivity of OSSE is only $2 \cdot 10^{-7}$ photons/(cm$^2 \cdot$ s $\cdot$ keV) (Gehrels & Shrader 1996). In the observations reported by Kuiper et al. (1996) the flux from Geminga in the band of 3–10 MeV was found to be $10^{-7}E_6^{-2}$ photons/(cm$^2 \cdot$ s $\cdot$ keV). Substituting Geminga parameters ($P = 0.237$ s, $B_{12} = 3.3$, $d_3 = 0.15$) into Eq. (19) one can obtain the flux provided by the upscattered Compton photons: $F = 3.8{\cdot}10^{-7}\kappa_3\gamma_3R_6^{5/2}E_6^{-2}$ photons/(cm$^2 \cdot$ s $\cdot$ keV), which is consistent with the one detected.

5. Conclusions

We have investigated resonant inverse Compton scattering by secondary pulsar plasma. The process is found to cause the efficient energy loss of the secondary particles given the neutron star temperatures $> 10^5$ K, so that our results are applicable to most pulsars. For the resonant character of the scattering, the energy loss depends strongly on the initial particle energy. At $\gamma_0 \sim 10^2 - 10^3$ the scattering is the most essential, the final Lorentz-factors of the particles being independent of the initial ones.

The distribution function of the secondary plasma is significantly altered by the resonant inverse Compton scattering. It is shown that ultimately the distribution function becomes two-humped. The main peak at $\gamma \lesssim 10^2$ is very sharp. It is formed by particles which suffered severe energy loss on account of the scattering. Another hump is sufficiently broad. It is associated with the particles, whose Lorentz-factors are almost unaltered by the scattering. The two-humped distribution function of the plasma particles is known to be unstable. It is shown that at pulsar conditions the two-stream instability develops readily and leads to an essential increase of plasma oscillations, which are likely to be transformed into radio emission.

We have also estimated the gamma-ray flux provided by the upscattered Compton photons. The resonantly scattered photons appear to gain the energies of 1–10 MeV forming an additional low-energy component in pulsar gamma-ray spectrum.

References

Alpar M.A., Anderson P.W., Pines D., Shaham J., 1984, ApJ 278, 791
Arons J., 1980, In: Sieber W., Wielebinski R. (eds.) Proc. IAU Symp. 95, Pulsars: 13 Years of Research on Neutron Stars. p. 69
Arons J., 1981, ApJ 248, 1099
Arons J., Scharlemann E.T., 1979, ApJ 231, 854
Becker W., Trumper J., 1993, Nat 365, 528
Benford G., Buschauer R., 1977, MNRAS 179, 189
Buschauer R., Benford G., 1977, MNRAS 179, 99
Chang H.-K., 1995, A&A 301, 456
Cheng A.F., Ruderman M.A., 1977, ApJ 212, 800
Cheng A.F., Ruderman M.A., 1980, ApJ 235, 576
Cordova F.A., Hjellming R.M., Mason K.O., Middleditch J., 1989, ApJ 345, 451
Daugherty J.K., Harding A.K., 1989, ApJ 336, 861
Dermer C.D., 1990, ApJ 360, 214
Finley J.P., Ogelman H., Kiziloglu U., 1992, ApJ 394, L21
Gehrels N., Shrader C.R., 1996, A&AS 120, 1
Greiveldinger C., Camerini U., Fry W. et al., 1996, ApJ 465, L35
Halpern J.P., Holt S.S., 1992, Nat 357, 222
Halpern J.P., Ruderman M.A., 1993, ApJ 415, 286
Herold H., 1979, Phys. Rev. D. 19, 2868
Kardashev N.S., Mitrofanov I.G., Novikov I.D., 1984, SvA 28, 651
Kuiper L., Hermsen W., Bennet K. et al., 1996, A&AS 120, 73
Lominadze D.G., Mikhailovskii A.B., 1979, ZETPh 76, 959
Luo Q., 1996, ApJ 468, 338
Lyubarskii Yu.E., 1993, Pis'ma v Astron. Zh. 19, 34
Lyubarskii Yu.E., 1995, Astrophys. & Space Phys. Rev. 9, pt.2, 1
Ogelman H., 1991, In: Ventura J., Pines D. (eds.) Neutron Stars: Theory and observation. p. 87
Ogelman H., 1995, In: Alpar M.A., Kiziloglu U., van Paradijs J. (eds.) The Lives of Neutron Stars. p. 101
Ogelman H., Finley J.P., 1993, ApJ 413, L31
Ogelman H., Finley J.P., Zimmerman H.U., 1993, Nat 361, 136
Page D., Applegate J.H., 1992, ApJ 394, L17
Qiao G.J., Zhang B., 1996, A&A 306, L5
Ruderman M.A., Sutherland P.G., 1975, ApJ 196, 51
Shibazaki N., Lamb F.K., 1989, ApJ 346, 808
Sturner S.J., 1995, ApJ 446, 292
Umeda H., et al., 1993, ApJ 408, 186
Usov V.V., 1987, ApJ 320, 333
Ursov V.N., Usov V.V., 1988, Ap&SS 140, 325
Van Riper K.A., 1991, ApJS 75, 449
Xia X.Y., Qiao G.J., Wu X.J., Hou Y.Q., 1985, A&A 152, 93
Yancopoulos S., Hamilton T.T., Helfand D.J., 1994, ApJ 429, 832
Zhang B., Qiao G.J., 1996, A&A 310, 135
Zhang B., Qiao G.J., Han J.L., 1997, ApJ 491, 891